Journal of Solid State Chemistry 182 (2009) 2456–2460

Contents lists available at ScienceDirect

Journal of Solid State Chemistry

journal homepage: www.elsevier.com/locate/jssc

Preparation of iron oxides using ammonium iron citrate precursor: Thin films and nanoparticles

Sangmoon Park [a,b,c,*]

[a] Department of Engineering in Energy and Applied Chemistry, Silla University, Busan 617-736, Republic of Korea[1]
[b] USC NanoCenter, Department of Chemistry and Biochemistry, University of South Carolina, 1212 Greene Street, Columbia, SC 29208-0001, USA[2]
[c] Condense Matter Physics and Materials Science Department, Brookhaven National Laboratory, Upton, NY 11973-5000, USA[2]

ARTICLE INFO

Article history:
Received 8 March 2009
Received in revised form
16 June 2009
Accepted 17 June 2009
Available online 24 June 2009

Keywords:
Iron oxides
Thin films
Nanoparticles
Transmission electron microscopy
Magnetic measurements

ABSTRACT

Ammonium iron citrate ($C_6H_8O_7 \cdot n$Fe$\cdot n H_3N$) was used as a precursor for preparing both iron-oxide thin films and nanoparticles. Thin films of iron oxides were fabricated on silicon (111) substrate using a successive-ionic-layer-adsorption-and-reaction (SILAR) method and subsequent hydrothermal or furnace annealing. Atomic force microscopy (AFM) images of the iron-oxide films obtained under various annealing conditions show the changes of the micro-scale surface structures and the magnetic properties. Homogenous Fe_3O_4 nanoparticles around 4 nm in diameter were synthesized by hydrothermal reduction method at low temperature and investigated using transmission electron microscopy (TEM).

1. Introduction

Iron oxides (Fe_2O_3 and Fe_3O_4) are technologically important materials engaged in the gas sensors [1–5], tunneling magnetoresistance (TMR) [6,7], recording medium [8,9], biocompatibility [10–13], and medical application [10,14]. A variety of deposition methods like molecular-beam epitaxy (MBE) [15], sputtering [6], pulsed laser deposition (PLD) [16,17], metallo-organic deposition (MOD) [18], plasma enhanced chemical vapor deposition (PECVD) [19], and atomic layer deposition (ALD) [20] have been widely used to fabricate iron-oxide films. It was shown that many metal-oxide films have been accomplished, using the successive-ionic-layer-adsorption-and-reaction (SILAR) deposition as a low-cost and simple fabrication technique [21–23]. Moreover, the combination of SILAR deposition followed by hydrothermal dehydration and annealing became a process for preparing homogenous and crystallized metal-oxide films at quite low temperature.

Nanoscale materials in applied single-electron devices, catalysts, and optical/electrical/magnetic devices have been intensively studied and such nanomaterials have been synthesized by using hydrothermal and reduction process [24–29]. The heterogeneous reaction in the presence of aqueous solvent or mineralizers under high pressure and high temperature leads to insoluble materials due to their dissolution–recrystallization process [30]. The reduction route refers to gaining electrons in process from reducing agent on the basis of the value of standard Gibbs free energy change (ΔG^0). The hydrothermal synthesize of magnetite (Fe_3O_4) and maghemite (γ-Fe_2O_3) nanoparticles at a low temperature have been used [31–35]. Iron nitrate 9-hydrate and ferrocene for synthesizing iron-oxide nanoparticles were specially utilized as iron precursors along with surfactants as well as reducing agent (hydrazine) [31,32]. Furthermore, a $(NH_4)_2SO_4 \cdot FeSO_4 \cdot 6H_2O$ precursor only in the presence of hydrazine was also exploited for the formation of iron oxides [33].

I herein report both the fabrication of iron-oxide films and synthesis of iron-oxide nanoparticles using ammonium iron citrate as a complexing precursor. The deposition and crystallization of iron-oxide films on the use of SILAR method followed by hydrothermal and/or furnace annealing were performed. The surface topography of iron-oxide films was investigated by AFM images, and their magnetic susceptibility (χ) as a function of field (H) was attained as well. A simple hydrothermal-reduction process at 150 °C was used for synthesizing homogenous iron-oxide nanoparticles about 4 nm in diameter.

2. Experimental details

Iron-oxide films on Si (111) substrate were prepared using aqueous solutions of 0.15 g ammonium iron citrate ($C_6H_8O_7 \cdot n$Fe$\cdot n H_3N$ Alfa, 99.998%) and 0.03 M NaOH (Analytical

* Corresponding author at: Department of Engineering in Energy and Applied Chemistry, Silla University, Busan 617-736, Republic of Korea.
Fax: +82 51 999 5806.
E-mail address: spark@silla.ac.kr
[1] Current address.
[2] Previous address.

0022-4596/$ - see front matter © 2009 Elsevier Inc. All rights reserved.
doi:10.1016/j.jssc.2009.06.027

Reagent). The substrates were attached to the arm of a Gilson 223 XYZ robotic sample changer and immersed in the Fe-complexing solution, water, NaOH solution, and water for 0.03, 0.06, 0.03, and 0.096 min (700 cycles), respectively. The water prepared in the use of a Millipore Milli-Q Academic™ ion-exchange system was vigorously stirred near the substrate using a magnetic stir bar in rinse bath. As-made films were cut into four pieces and then each piece of film was transferred to a sealed Teflon-lined Parr Reactor™. The films were hydrothermally heated at 200 °C, directly annealed in air at 600 °C, or annealed under 4% H_2/Ar at 600 °C in a furnace. X-ray diffraction measurements using Cu$K\alpha$ radiation were done using a MiniFlex$^+$ (Rigaku) diffractometer. The surface topography was examined with a NanoScopeII atomic force microscopy (AFM, tapping mode). Magnetization measurements were carried out using a SQUID magnetometer in the temperature at 300 K at applied fields 20 kOe$\leq H \leq -20$ kOe.

For the synthesis of iron-oxide nanoparticles, 5 mL distilled water was added to a Teflon-lined Parr reactor™ in a capacity of 23 mL and then 0.02 g ammonium iron citrate precursor was dissolved in water with stirring for 15 min. Finally, 3 mL $N_2H_4 \cdot H_2O$ was slowly added to the solution. The solution was sealed in an autoclave and maintained at 150 °C for 18 h. When the reaction was finished, the black-solid products were obtained. The products were washed with ethanol using a centrifuge and then stored in ethanol to prevent oxidation. Transmission electron microscopy (Hitachi H-8000, 200 kV) was used for the typical morphologies of iron-oxide nanoparticles.

3. Results and discussion

The SILAR method could be one of the thin film deposition techniques in addition to a variety of iron-oxide fabrication methods as described above. It is essential to choose a metal cation constituent for preparing homogenous films in point of SILAR deposition method. Iron nitrate 9-hydrate could be utilized for the one of typical iron-oxide precursors. For preparing iron-oxide nanoparticles, the precursor needs to be used with complex surfactant species like sodium bis(2-ethylhexly)sulfosuccinate, and moreover, it is known as a hydroscopic chemical as well as an acidic reagent, when dissolved in water. The ammonium iron citrate was selected as a cation constituent, NH_4^+[Fe(OH)citrate]$^-$. Its advantages over the common precursor are that this simple complex precursor can diminish the rapid aggregations of metal cation and hydroxide anion without a surfactant, it can be handled easily in air, and Fe-complexing in solution showing the mild pH (~5) can be gently precipitated with anions (OH^-) along with a potential/pH diagram, a pourbaix diagram. All films were characterized by X-ray powder diffraction to identify the iron-oxide phases present. The ICSD data (α-Fe_2O_3 22505, Fe_3O_4 30860, γ-Fe_2O_3 79196) were used for indexing the observed iron-oxide phases shown in Fig. 1(a–f). XRD patterns of Fe_3O_4 and γ-Fe_2O_3 are intricate to distinguish two phases even though they have different space groups, $Fd3m$ for Fe_3O_4 and $P4_332$ for γ-Fe_2O_3. Furthermore, both oxides show ferromagnetic behavior in magnetic property [36]. The broad Si (111) substrate peak on all films was observed around $2\theta = 28 \sim 29$ in Fig. 1(d–f). The (311) γ-Fe_2O_3 (or Fe_3O_4) peak (*) around $2\theta \sim 35.9$ was observed from XRD patterns (Fig. 1(d) and (f)) of both films annealed by hydrothermal dehydration and under reduction environment. When the films were annealed in air, the (104) and (110) α-Fe_2O_3 peaks (●) around $2\theta \sim 33.4$, 35.8 were obtained in Fig. 1(e).

Fig. 2 shows the AFM images and the partial magnetic curves of iron-oxide films, which were (a) as-deposited, (b) hydrothermally dehydrated and annealed at 200 °C, (c) furnace annealed in air at 600 °C, and (d) under 4% H_2/Ar at 600 °C,

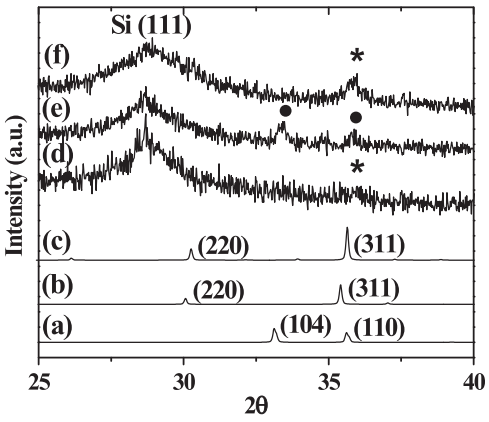

Fig. 1. X-ray diffraction patterns of calculated: (a) α-Fe_2O_3 (ICSD 22505), (b) Fe_3O_4 (ICSD 30860), (c) γ-Fe_2O_3 (ICSD 79196) and observed iron-oxide thin films (d) hydrothermal at 200 °C, (e) in air at 600 °C and (f) under 4% H_2/Ar at 600 °C.

respectively. The 3D views at the 5 μm scale AFM images are shown in Fig. 2. Cross-sectional scanning electron microscopy of as-made films revealed thickness not greater than 150 nm that is not shown in this report. Like ZrO_2 [21], CeO_2 [22], and TiO_2 [23] films prepared by SILAR technique, the as-deposited iron-oxide films reveal similar results of homogenously closely packed nanoparticles with approximately 25 nm diameters. In accordance with the broad XRD peaks of the iron-oxide films annealed hydrothermally at 200 °C in Fig. 1(d), the homogenous nanoparticles on the films are observed by the AFM image in Fig. 2(a). The grain morphology of the furnace annealed iron-oxide films in air or under H_2/Ar at 600 °C occurs much bigger than the one observed in hydrothermally annealed films. As shown in Fig. 2(c) and (d), the grain morphology of the furnace annealed iron-oxide films at 600 °C is a couple of hundred nanometers large, showing substantial surface roughness. The partial demagnetization curves for iron-oxide films were plotted at 300 K. The demagnetization curves for the as-made films (Fig. 2(a)) and furnace-annealed films in air at 600 °C (Fig. 2(c)) were perturbed downwards by 20 kOe. While the curve for hydrothermal annealed films exhibits an unsaturated magnetism, the curve for furnace-annealed films under H_2/Ar at 600 °C shows a saturated magnetism around 500 Oe. These films annealed under reducing environment (H_2/Ar) might be magnetic γ-Fe_2O_3 or Fe_3O_4, which have two oxidation valence states (Fe^{2+} and Fe^{3+}). The iron-oxide films annealed in air at 600 °C show diamagnetic behavior, and thus they are non-magnetic α-Fe_2O_3 films, which have an oxidation valence state (Fe^{3+}). Interestingly, when as-made films were hydrothermally annealed at 200 °C, the iron-oxide films show superparamagnetic behavior due to that the coercive force is negligible as shown in Fig. 2(b) [31]. The iron-oxide films at a low temperature (200 °C) were not fully capable of being transformed to α-Fe_2O_3 phase due to the lack of oxygen sources in sealed hydrothermal vessel. When as-deposited films with water as an oxygen source were placed in the hydrothermal reactor, the phase of iron oxides was clearly transformed to α-Fe_2O_3. It is associated with the presence of a sufficient oxygen source (water) to oxidize the films. In the cubic inverse spinel Fe_3O_4 structure, Fe^{3+} ions occupy tetrahedral and octahedral sites and Fe^{2+} ions are in tetrahedral site. It is known that the aligned antiparallel spins of Fe^{3+} ions, which occupy octahedral and tetrahedral sites, lead magnetic moment [37,38]. The unsaturated magnetic behavior observed in hydrothermally annealed films at 200 °C is attributed to the lack of the formation of the magnetic domains. However, the furnace-annealed films under reducing environment show the saturated magnetic

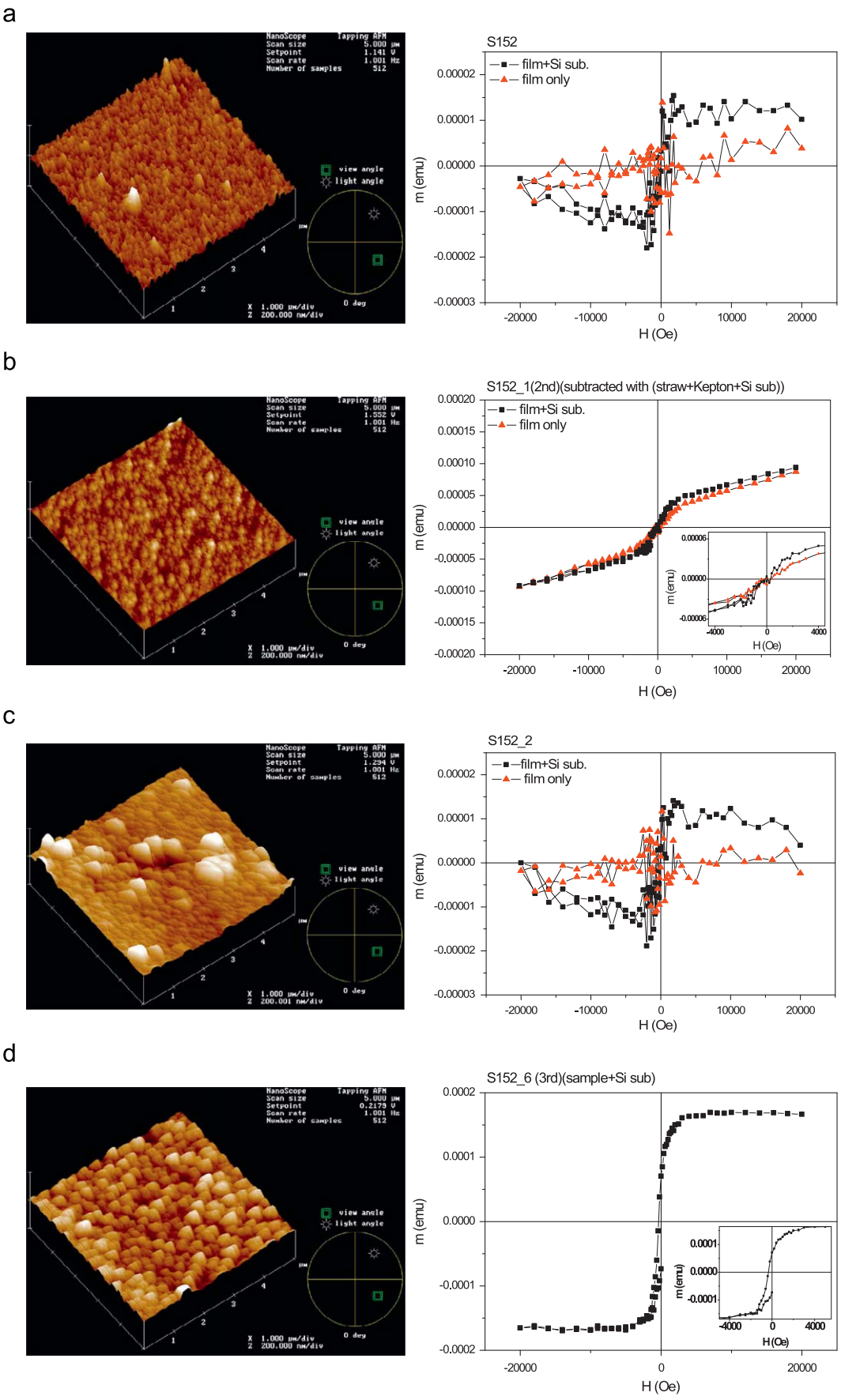

Fig. 2. AFM images and the partial magnetic curves (the inset *M*–*H* data corresponds to *H* from −4 to 4 kOe) of iron oxides: (a) as-deposited, (b) hydrothermal annealed at 200 °C, (c) furnace annealed in air, (d) under 4% H_2/Ar at 600 °C.

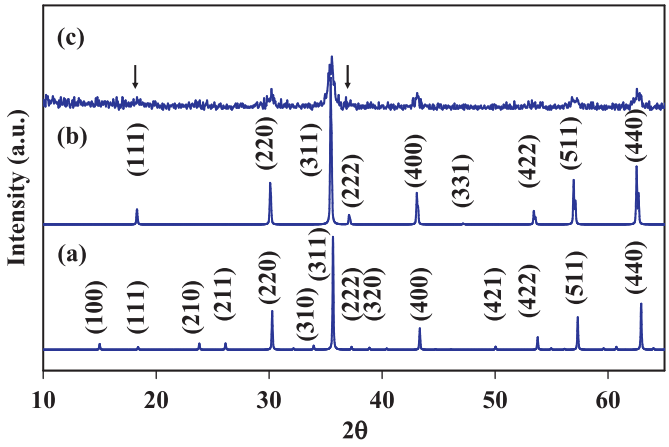

Fig. 3. X-ray diffraction patterns of calculated (a) γ-Fe_2O_3 (ICSD 79196), (b) Fe_3O_4 (ICSD 30860) and observed (c) Fe_3O_4 nanoparticles.

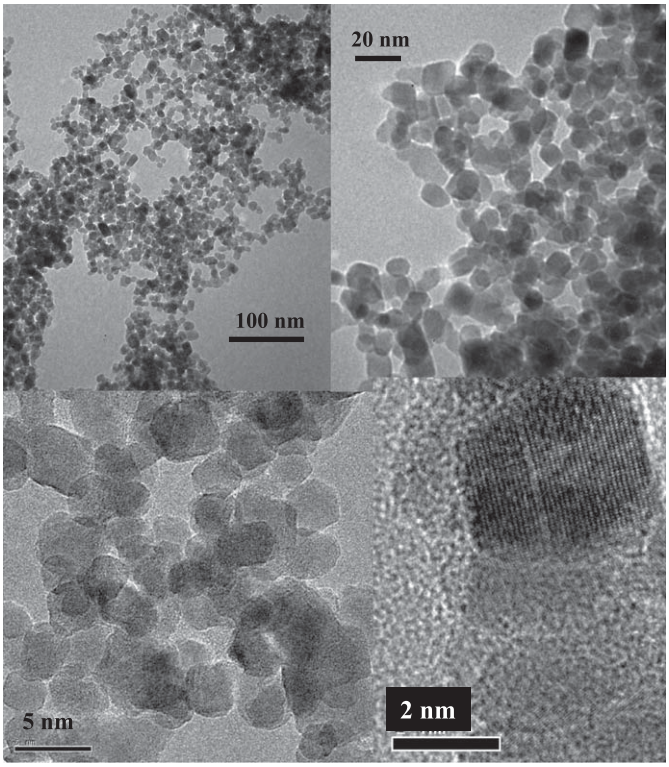

Fig. 4. TEM image of Fe_3O_4 nanoparticles.

behavior because the energy barriers can be overcome when films were heated at a high temperature (600 °C).

As mentioned above, nanosized iron oxides have been synthesized using various precursors in the hydrothermal reduction method. The ammonium iron citrate as a precursor for preparing iron-oxide nanoparticles was not used previously, to my knowledge. The ammonium iron citrate is easy to dissolve in water (NH_4^+[Fe(OH)citrate]$^-$) presenting mild pH~5, and moreover, this complex precursor can play a role of a surfactant during hydrolysis process to form homogeneous nanoparticles. When the ammonium iron citrate was dissolved in water, $N_2H_4 \cdot H_2O$ was slowly added to the solution. The color of solution turned into black from colorless. The hydrothermal reduction process at 150 °C using a Teflon-lined Parr reactor™ was performed. Black solid products were attained after the reaction. The product was characterized by X-ray powder diffraction for phase identification as shown in Fig. 3. In X-ray diffraction patterns, five intense peaks are indexed by (220), (311), (400), (511), and (440), which are matched with Fe_3O_4 and γ-Fe_2O_3 phases. The relatively broad peaks (↓) around 2θ~18.5, 37.5 are indexed by (111), (222) Fe_3O_4 diffractions. It is hard to tell apart whether the product is Fe_3O_4 or γ-Fe_2O_3 phase, but the X-ray diffraction analysis indicates that possibly it is close to Fe_3O_4 nanoparticles. No preferred orientation from the powder X-ray diffraction of Fe_3O_4 nanoparticles was detected.

Transmission electron microscopy (TEM) provides the typical morphologies of as-synthesized Fe_3O_4 in Fig. 4. TEM images indicate a very uniform size distribution of Fe_3O_4 nanoparticles. Previously, the size-controlled synthesis for magnetic Fe_3O_4 nanoparticles was performed for the first time in the use of Fe(*acac*)$_3$ in phenyl ether, alcohol, oleic acid, and oleylamine [39]. In this work, Fe_3O_4 nanoparticles around 4 nm in diameter (Fig. 4) were also able to be generated by the use of ammonium iron citrate precursor, hydrazine, and water. Using the hydrothermal reduction method, the synthesis of homogeneous Fe_3O_4 nanoparticles doped with metals such as Au, Ag, or Pt applying to the biomedical purpose is underway.

4. Conclusions

Ammonium iron citrate was readily chosen as a precursor to fabricate iron-oxide films and prepare nanoparticles. Iron-oxide films were successfully deposited on Si wafer using SILAR method. As the results of XRD and magnetic investigations, the γ-Fe_2O_3 or the Fe_3O_4 phase was obtained by hydrothermal or furnace-annealed (under H_2/Ar) films and α-Fe_2O_3 phase was achieved by furnace-annealed (in air) films. AFM images of iron-oxide films reveal different morphologies under various annealing conditions. Especially homogenous Fe_3O_4 nanoparticles about 4 nm in diameter were synthesized by hydrothermal reduction method, and the morphology was investigated by TEM.

Acknowledgments

I am grateful to Dr. T. Vogt and Dr. K. Kang for their fruitful discussions and help.

References

[1] L. Huo, W. Li, L. Lu, H. Cui, S. Xi, J. Wang, B. Zhao, Y. Shen, Z. Lu, Chem. Mater. 12 (2000) 790.
[2] O.K. Tan, W. Zhu, Q. Yan, L.B. Kong, Sens. Acutators B 65 (2000) 361.
[3] N. Yamazoe, N. Miura, Sens. Acutators B 20 (1994) 95.
[4] W. Göpel, Sens. Acutators B 18–19 (1994) 1.
[5] M. Matsuoka, Y. Nakatani, H. Ohido, Natl. Tech. Rep. 24 (1978) 461.
[6] Y. Peng, C. Park, D.E. Laughlin, J. Appl. Phys. 93 (2003) 7957.
[7] K.-I. Aoshima, S.X. Wang, J. Appl. Phys. 93 (2003) 7954.
[8] W. Yi, W. MoberlyChean, V. Narayanamurit, Y.F. Hu, Q. Li, I. Kaya, M. Burns, D.M. Chen, J. Appl. Phys. 95 (2004) 7136.
[9] J.C. Mallinson, The Foundations of Magnetic Recording, Academic, Berkeley, 1987.
[10] Y. Qiang, J. Antony, M.G. Marino, S. Pendyala, IEEE Trans. Magn. 40 (2004) 3538.
[11] D.K. Kim, M. Mikhaylova, Y. Zhang, M. Muhammed, Chem. Mater. 15 (2003) 1617.
[12] M. Tada, S. Hatanaka, H. Sanbonsugi, N. Matsushita, M. Abe, J. Appl. Phys. 93 (2003) 7566.
[13] M. Chen, S. Yamamuro, D. Farrell, S.A. Majetich, J. Appl. Phys. 93 (2003) 7551.
[14] U. Häfeli, W. Schütt, J. Teller, M. Zborowski, Scientific and Clinical Application of Magnetic Carriers, Plenum Press, New York, 1997.
[15] D.M. Lind, S.M. Berry, G. Chern, H. Mathias, L.R. Testardi, Phys. Rev. B 45 (1992) 1838.
[16] C.A. Klient, H.C. Semmelhack, M. Lorenz, M.K. Krause, J. Magn. Magn. Mater. 725 (1995) 140.
[17] W.L. Zhou, K.-Y. Wang, C.J. O'Connor, J. Tang, J. Appl. Phys. 89 (2001) 7398.
[18] S. Xue, W. Ousi-Benomar, R.A. Lessard, Thin Solid Films 250 (1994) 194.

[19] Y. Liu, W. Zhu, O.K. Tan, Y. Shen, Mater. Sci. Eng. 47 (1997) 171.
[20] O. Nilsen, M. Lie, S. Foss, H. Fjellvag, A. Kjekshus, Appl. Surf. Sci. 227 (2004) 40.
[21] S. Park, B.L. Clark, D.A. Keszler, J.P. Bender, J.F. Wager, T.A. Reynolds, G.S. Herman, Science 297 (2002) 65.
[22] S. Park, G.S. Herman, D.A. Keszler, J. Solid State Chem. 175 (2003) 84.
[23] S. Park, E. DiMasi, Y.-I. Kim, W. Han, P.M. Woodward, T. Vogt, Thin Solid Films 515 (2006) 1250.
[24] Y. Jin, K. Tang, C. An, L. Huang, J. Crystal Growth 253 (2003) 429.
[25] Y. Li, J. Wang, Z. Deng, Y. Wu, X. Sun, D. Yu, P.J. Yang, Am. Chem. Soc. 123 (2001) 9904.
[26] H. Liu, J.Y. Wang, X.B. Hu, F. Gu, L. Hua, C.Q. Zhang, B. Tneg, D.L. Cui, J.Q. Pan, Chem. Mater. 13 (2001) 151.
[27] H.H. Nersisyan, J.H. Lee, H.T. Son, C.W. Won, D.Y. Maeng, Mater. Res. Bull. 38 (2003) 949.
[28] Q. Xie, Z. Dai, W. Hyang, J. Liang, C. Jiang, Y. Qian, Nanotechnology 16 (2005) 2958.
[29] S. Park, K. Kang, W. Han, T. Vogt, J. Alloys Compd. 400 (2005) 88.
[30] K. Byrappa, M. Yoshimura, Handbook of Hydrothermal Technology: A Technology for Growth and Materials Processing, William Andrew Publishing, 2001 p. 7.
[31] Y.-H. Zheng, Y. Cheng, F. Bao, Y.-S. Wang, Mater. Res. Bull. 41 (2006) 525.
[32] G. Zou, K. Xiong, C. Jiang, H. Li, T. Li, J. Du, Y. Qian, J. Phys. Chem. 109 (2005) 18356.
[33] Y. Li, H. Liao, Y. Qian, Mater. Res. Bull. 33 (1998) 841.
[34] D. Chen, R. Xu, J. Solid State Chem. 137 (1998) 185.
[35] T.J. Daou, G. Pourroy, S. Bégin-Colin, J.M. Grenéche, C. Ulhaq-Bouillet, P. Legaré, P. Bernhardt, C. Leuvrey, G. Rogez, Chem. Mater. 18 (2006) 4399.
[36] F. Jiao, J.-C. Jumas, M. Womes, A.V. Chadwick, A. Harrison, P.G. Bruce, J. Am. Chem. Soc. 128 (2006) 12905.
[37] S.K. Arora, H.-C. Wu, R.J. Choudhary, I.V. Shvets, O.N. Mryasov, H. Yao, W.Y. Ching, Phys. Rev. B 77 (2008) 134443.
[38] F.C. Voogt, T.M. Palstra, L. Niesen, O.C. Rogojanu, M.A. James, T. Hibma, Phys. Rev. B 57 (1998) R8107.
[39] S. Sun, H. Zeng, J. Am. Chem. Soc. 124 (2002) 8204.